Fine and distributed subcellular retinotopy of excitatory inputs to the dendritic tree of a collision-detecting neuron

Ying Zhu and Fabrizio Gabbiani

J Neurophysiol 115:3101-3112, 2016. First published 23 March 2016;
doi: 10.1152/jn.00044.2016

J Neurophysiol 115: 3101–3112, 2016.
First published March 23, 2016; doi:10.1152/jn.00044.2016.

Fine and distributed subcellular retinotopy of excitatory inputs to the dendritic tree of a collision-detecting neuron

Ying Zhu and Fabrizio Gabbiani

Department of Neuroscience and Program of Structural and Computational Biology and Molecular Biophysics, Baylor College of Medicine, Houston, Texas

Submitted 16 January 2016; accepted in final form 21 March 2016

Zhu Y, Gabbiani F. Fine and distributed subcellular retinotopy of excitatory inputs to the dendritic tree of a collision-detecting neuron. *J Neurophysiol* 115: 3101–3112, 2016. First published March 23, 2016; doi:10.1152/jn.00044.2016.—Individual neurons in several sensory systems receive synaptic inputs organized according to subcellular topographic maps, yet the fine structure of this topographic organization and its relation to dendritic morphology have not been studied in detail. Subcellular topography is expected to play a role in dendritic integration, particularly when dendrites are extended and active. The lobula giant movement detector (LGMD) neuron in the locust visual system is known to receive topographic excitatory inputs on part of its dendritic tree. The LGMD responds preferentially to objects approaching on a collision course and is thought to implement several interesting dendritic computations. To study the fine retinotopic mapping of visual inputs onto the excitatory dendrites of the LGMD, we designed a custom microscope allowing visual stimulation at the native sampling resolution of the locust compound eye while simultaneously performing two-photon calcium imaging on excitatory dendrites. We show that the LGMD receives a distributed, fine retinotopic projection from the eye facets and that adjacent facets activate overlapping portions of the same dendritic branches. We also demonstrate that adjacent retinal inputs most likely make independent synapses on the excitatory dendrites of the LGMD. Finally, we show that the fine topographic mapping can be studied using dynamic visual stimuli. Our results reveal the detailed structure of the dendritic input originating from individual facets on the eye and their relation to that of adjacent facets. The mapping of visual space onto the LGMD's dendrites is expected to have implications for dendritic computation.

lobula giant movement detector; descending contralateral movement detector; looming; collision avoidance; locust

NEW & NOTEWORTHY

The lobula giant movement detector (LGMD), a model neuron for dendritic computation implicated in collision avoidance behavior, receives a retinotopic, distributed projection from each ommatidium (facet) on the eye. Most of the branches activated by a single facet have large dendritic separations. Adjacent facets exhibit overlapping input patterns, but most likely from independent synapses onto single excitatory dendrites of the LGMD.

TOPOGRAPHIC MAPPINGS ARE UBIQUITOUS in sensory systems. They have been widely studied on a population level in different species, for example, in the mammalian primary visual cortex (Adams and Horton 2003; Gias et al. 2005; Schuett et al. 2002), the auditory system of barn owls (Knudsen and Konishi 1978), and the electrosensory system of weakly electric fish (for review see Krahe and Maler 2014). At the subcellular level, studies using calcium imaging in neurons of the mammalian retina, the vertebrate optic tectum, and the insect visual system showed evidence of topographic dendritic input organization (Bollmann and Engert 2009; Euler et al. 2002; Hopp et al. 2014; Peron et al. 2009; Spalthoff et al. 2010). However, how the morphological structure of dendrites and the specifics of topographically organized synaptic inputs influence synaptic integration and dendritic computation remains largely unknown.

The lobula giant movement detector (LGMD) is a large visual interneuron in the third neuropil of the optic lobe of orthopteran insects (O'Shea and Williams 1974). Being most sensitive to objects approaching on a collision course with the animal or their two-dimensional simulations (i.e., looming stimuli; Hatsopoulos et al. 1995; Rind and Simmons 1992; Schlotterer 1977), the LGMD neuron plays an important role in visually evoked escape behavior (Fotowat and Gabbiani 2011; Santer et al. 2006). The LGMD's output spikes are coupled 1:1 with those of its postsynaptic target, the descending contralateral movement detector (DCMD), which has the largest axon in the locust nerve cord and projects to thoracic motor centers, where it makes synapses with identified motor neurons and interneurons implicated in the generation of jump and flight (Burrow and Rowell 1973; O'Shea and Williams 1974). Each adult locust compound eye consists of ~7,500 ommatidia (facets) and samples visual input from an entire visual hemifield. The orientation of the optical axes of each individual ommatidium has been directly measured (Krapp and Gabbiani 2005). Because the locust eye is of the apposition type (Shaw 1969), each facet represents the elementary sampling unit of the eye and determines its finest level of spatial resolution.

The LGMD neuron is a model for dendritic computation (Dewell and Gabbiani 2016; Gabbiani et al. 2002) that has been shown to receive retinotopic inputs from the ipsilateral compound eye on its excitatory dendritic field through calcium-permeable nicotinic acetylcholine receptors (Peron et al. 2009). The study by Peron et al. (2009) employed wide-field CCD camera imaging with a relatively low penetration depth and spatial resolution. As a consequence, fine-scale retinotopy was revealed indirectly through statistical arguments. In addition, this study used a projection screen to present visual stimuli of a size similar to that of single photoreceptors' receptive fields. As a consequence, because of the uncertainty in the stimulated location on the eye this work could not study retinotopy in fine detail. Because of these limitations, several important questions remained to be answered. How do synaptic

Address for reprint requests and other correspondence: F. Gabbiani, Baylor College of Medicine, 1 Baylor Plaza, MS-BCM295 Houston, TX 77030 (e-mail: gabbiani@bcm.edu).

inputs from individual ommatidia or facets wire onto the LGMD? What is the spatial organization of the synaptic locations activated by adjacent facets? Do synaptic inputs from multiple facets sum linearly on the dendrites? To answer these questions, we employed a custom single-facet stimulation setup in conjunction with two-photon calcium imaging of the excitatory dendrite of the LGMD. This stimulus-recording configuration provided the highest possible spatial resolution both in terms of the sensory input activated on the eye and in terms of in vivo spatial resolution during functional dendritic imaging.

In this work, we begin by directly demonstrating that single-facet stimuli elicit extended and distributed activation patterns on the LGMD excitatory dendrite. Next, we show that these distributed activation patterns are nonetheless highly orderly, because their centers of mass (COMs) preserve retinotopy at the finest level. Subsequently, we study how the activation of adjacent facets shapes the activation of dendritic compartments in the LGMD and the likely wiring strategy of the synaptic inputs originating from adjacent facets. Finally, we investigate the responses of the LGMD to local dynamic stimuli with simultaneous calcium and intracellular recordings.

MATERIALS AND METHODS

Preparation. Experiments were carried out on mature locusts (mostly female), 3–4 wk past the final molt, taken from a crowded colony maintained at Baylor College of Medicine. Animals were mounted dorsal side up on a custom holder. The head was rotated 90° with the anterior side pointing downward. The entire head and neck were bathed in ice-cold locust saline, except for the right eye used for visual stimulation. The gut was removed. The head capsule was opened dorso-frontally between the two eyes. The muscles in the head capsule were removed. The head was carefully detached from the body, leaving only the two nerve cords and four trachea attached. The right optic lobe was desheathed mechanically with fine forceps. A metal holder elevated and stabilized the brain and the right optic lobe. A typical dissection and animal preparation lasted 1.5 h.

Visual stimulation. Visual stimuli were generated with the Psychtoolbox and MATLAB (The MathWorks, Natick, MA). Individual facets (ommatidia) on the locust compound eye were stimulated with a setup similar to that employed previously (Fig. 1*A*; Jones and Gabbiani 2010). Instead of using a video projector, we used a miniature organic light-emitting diode (OLED) display (800 × 600 pixels, 60 Hz refresh rate; OLiGHTEK SVGA050SG). The low refresh rate of the display was not a limitation for the present experiments since individual facets were mainly activated with constant steps in luminance. Even in the case of looming stimuli, similar refresh rates have been shown to minimally affect LGMD responses (Gabbiani et al. 1999). Each single-facet visual stimulus was an "OFF" flash lasting 50 ms subtending a size of 22 μm at the retina and focused at the center of an ommatidium on the compound eye (Fig. 1*B*; ommatidium diameter: ~24 μm). The brightness of the display before and after the flash was 72.43 cd/m^2. The brightness of the screen at the level used for "OFF" stimuli was 1.63 cd/m^2. The brightness of the screen was calibrated by a photometer and linearized by loading a normalized gamma table to the Psychtoolbox. The single-facet stimulation setup was mounted horizontally, perpendicular to the two-photon imaging objective lens or tilted by 4° or 8° with respect to the horizontal to stimulate the facets located more posteriorly on the compound eye. The space between the animal's right eye and the horizontally positioned objective lens (×10/0.3 NA, water immersion; CFI Plan Fluor 10XW, Nikon Instruments, Melville, NY) was submerged in water to neutralize the lenses of each ommatidium that have a similar refractive index (Franceschini and Kirschfeld 1971). The objective was focused onto the photoreceptors' plane behind the cornea that was visualized with a ring light mounted on the objective.

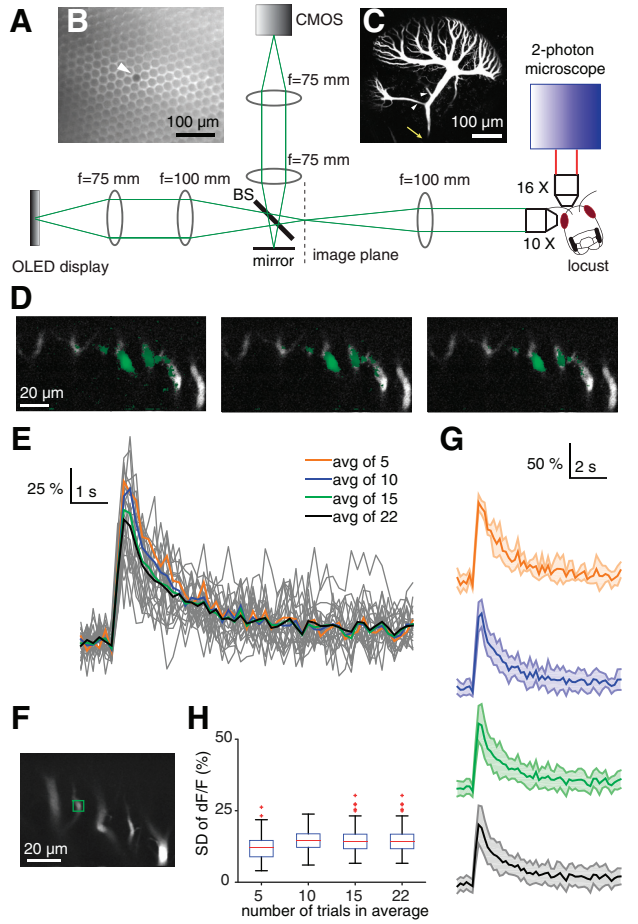

Fig. 1. Single-facet stimulation setup and custom 2-photon microscope. *A*: optical diagram of the single-facet stimulation setup. The OLED display generated the visual stimulus. A pellicle beamsplitter (BS) reflects half of the light beam from the eye and half from the OLED display, which are simultaneously focused on the CMOS camera sensor. The focal length of the 5 lenses (gray ellipses) is indicated by f. *B*: sample image of the compound eye taken by the CMOS camera. The darker facet (ommatidium, arrowhead) at the center is being stimulated with an OFF-stimulus. *C*: sample image of the maximal *z*-projection of a LGMD stain. As evidenced in this image, dendritic field A exhibits elaborate dendritic branching. The primary branches of fields B and C are also visible (arrowheads), and the approximate location of the spike initiation zone is indicated by the yellow arrow. *D*: comparison of the effect of different threshold levels on calcium activity maps. *Left*, *center*, and *right* show the pixels with peak dF/F values larger than 120%, 150%, and 180% of the maximum noise, respectively. Note that only pixels within dendritic segments are activated with the highest threshold. *E*: 22 trials (shown in gray) of the spatially averaged dF/F within the selected portion of the dendritic branch illustrated in *F* in response to a single-facet stimulation (spatial average over green rectangle). The averages of the first 5, 10, 15, and 22 trials are plotted in orange, blue, green, and black, respectively. *F*: region of interest (green) used in *E*, *G*, and *H*. *G*: orange, blue, green, and black traces in *E* are replotted with the standard deviations (SDs) shown by shading. *H*: box plot of the SD of dF/F at each frame as a function of the number of trials included in the average (each trial has 55 frames).

Staining. At the beginning of an experiment, the LGMD neuron was impaled with a sharp intracellular electrode (230–300 MΩ) containing 3 μl of 2 M potassium chloride and 1 μl of 5 mM Oregon Green BAPTA-1 (OGB1, hexapotassium salt; Thermo Fisher Scientific, Waltham, MA). Iontophoresis of OGB1 was achieved with current pulses of −3 nA, alternating between 1 s on and 1 s off, that

lasted for 6 min. The pulses were delivered by an Axoclamp 2B amplifier (Molecular Devices, Sunnyvale, CA). The LGMD was uniquely identified through its characteristic spike pattern in 1:1 correspondence with that of its postsynaptic target, the DCMD, recorded extracellularly from the nerve cord with hook electrodes.

Imaging, electrophysiology, and data acquisition. We employed a custom-built two-photon microscope based on a galvanometric scanning system (6215HSM40B; Cambridge Technology, Bedford, MA). The excitation wavelength was 820 nm, and the emission filter had a pass band between 500 and 550 nm (ET525/50M-2P; Chroma Technology, Bellow Falls, VT). The objective lens was a ×16/0.8 NA water immersion lens (CFI75 LWD 16XW; Nikon Instruments). The maximum scanning rate of the galvanometric mirrors was 23.68 frame/s with 32 lines/frame. Images of the LGMD excitatory dendritic field (Fig. 1*C*) were acquired by Scanimage software (r3.8, Vidrio Technologies, Arlington, VA) with a photon-counting photomultiplier tube (H7422P-40; Hamamatsu, Bridgewater, NJ). Five trials were averaged for each visual stimulus. For some dendritic branches that did not lie in a single horizontal plane, a stack of three to five images was taken while providing the same visual stimuli and *z* projections of the stacks were constructed (pixel-by-pixel summation).

Intracellular LGMD and extracellular DCMD recordings were performed simultaneously with two-photon calcium imaging in some animals. After identification of the location in the excitatory dendritic branches of the LGMD neuron that generated the calcium responses to the single-facet stimuli, a sharp electrode (25 MΩ) containing 3 μl of 2 M potassium chloride and 1 μl of 0.24 mM OGB1 was inserted into the excitatory dendrite of the LGMD for recording. Intracellular signals were amplified in bridge mode with an Axoclamp 2B and an instrumental amplifier (Brownlee Precision 440; NeuroPhase, Palo Alto, CA). LGMD and DCMD signals were acquired by Scanimage with a data acquisition card with a sampling rate of 0.19 MHz (PCI 6110; National Instruments, Austin, TX).

Data analysis and model of responses to dynamic stimuli. Data analysis was performed with MATLAB. The relative fluorescence change was calculated as $dF/F(t) = [F(t) - F_0]/F_0$ with the baseline fluorescence, F_0, being the average of the first five frames before the stimulus and the last five frames of the recording. For peak dF/F spatial maps, the $F(t)$ value at each pixel was the average over a 5 × 5-pixel area centered at the given pixel. After averaging, only suprathreshold pixels were used, defined as having a peak dF/F > 180% of the maximum noise of dF/F at that pixel. The maximum noise at each pixel was computed as the maximum of the dF/F values within 6 s before and well after the onset of the visual stimulus. The threshold value of 180% was selected in order to eliminate pixels resulting in falsely positive dF/F outside the dendritic branches (Fig. 1*D*). COMs were computed after pooling suprathreshold pixels across trials. To compute the dendritic distance between every two dendritic branches activated above threshold in response to a single-facet stimulus, we first performed a three-dimensional reconstruction of the two-photon image stacks of the whole LGMD excitatory dendrite in six animals and marked the shortest dendritic path connecting the centers of the activated regions on each pair of dendritic branches using Vaa3D (Peng et al. 2010, 2014a, 2014b). The marked dendritic paths were loaded to MATLAB, and the dendritic distances between each pair of activated branches were computed. When computing the area activated by the summed response of two single facets, we applied the threshold after summing the responses. If r_1 and r_2 denote the area activated by individual facets, while the area simultaneously activated by both facets is $r_{1\&2}$, we were interested in testing whether $r_1 + r_2 = r_{1\&2}$ (see Fig. 4). Because the threshold operation, denoted by $t(\cdot)$, is nondecreasing, we tested instead whether $t(r_1 + r_2) = t(r_{1\&2})$.

A first-order low-pass Butterworth filter with a cutoff equal to 0.08 times the frame rate was applied to the dF/F traces when comparing the dF/F in response to different speeds of luminance change. To analyze intracellular recordings, the LGMD membrane potential was first downsampled 50 times to 3.88 kHz and then median filtered within a time window of 8 ms to remove action potentials. A notch filter centered at 60 Hz was applied to remove the electrical noise (bandwidth: 8.8×10^{-4} Hz at −3 dB).

Using MATLAB, we implemented a simple model of the calcium responses to expanding dark disks illustrated in Fig. 8*G*. In these experiments, the stimuli expanded from the center of one facet to eventually cover three concentric layers of 1, 6, and 12 facets, respectively (Fig. 8*F*, *right*). The expansion either was instantaneous or occurred at a constant speed over an interval of 0.6 or 1.3 s (Fig. 8*G*, *top*). We assumed that the total calcium response, $f_T(t)$, was the linear sum of responses to individual facets, $f(t)$, according to the following equation:

$$f_T(t) = f(t) + 6a_1 f(t - \Delta t_1) + 12a_2 f(t - \Delta t_2) \quad (1)$$

We also assumed that the single-facet calcium response, $f(t)$, to moving edges was identical to the single-facet calcium response to an instantaneous luminance change. To constrain the values of a_1 and a_2, we employed the results depicted in Fig. 3, *I* and *J*. That is, since the overlap ratio between facets separated by one facet was ~0.5, we set $a_1 = 0.5$. Similarly, since the overlap ratio between facets separated by two facets was ~0.2, we set $a_2 = 0.2$. The delays Δt_1 and Δt_2 were set equal to the time delay between stimulus onset and the moment when the expanding edge started moving across the second and third facet layers, respectively. We obtained an estimate of $f(t)$ by setting Δt_1 and Δt_2 to 0 in *Eq. 1* and using the experimental data on the calcium response to an instantaneous luminance change over the three concentric layers (Fig. 8*G*, *bottom*, black curve). A prediction for expansions lasting $t_{ex} = 0.6$ and 1.3 s was then obtained from this $f(t)$ using $\Delta t_1 = t_{ex}/5$ and $\Delta t_2 = 3t_{ex}/5$ in *Eq. 1*.

Statistics. The number of trials acquired in each experiment was determined by a preliminary assessment of the influence of trial numbers on the average dF/F noise. There was no significant difference between the amplitude of dF/F averaged over 5 trials or 22 trials. The standard deviation computed over 22 trials was slightly bigger than that over 5 trials (Fig. 1, *E–H*).

For two-sample comparisons, we performed a nonparametric Mann-Whitney *U*-test. The null hypothesis was rejected and the results were judged statistically significant at probabilities $P < 0.05$.

To compare the size of the areas activated by either one or two facets stimulated simultaneously, as well as the summed area activated by two facets, we used a paired signed-rank test, which minimized interanimal and interfacet variability (see Fig. 4 and corresponding section in RESULTS).

The significance levels (*P* value) for the correlation coefficients in Fig. 8, *C* and *E*, were computed with the MATLAB function corrcoef.

RESULTS

The LGMD neuron possesses three dendritic fields (A–C), one of which receives excitatory synaptic inputs and is organized retinotopically (field A; O'Shea and Williams 1974; Peron et al. 2009). From anatomical studies, an estimated 15,000 afferent fibers supply these synaptic inputs (2 per facet; Strausfeld and Nässel 1981). To study the fine retinotopic mapping of visual inputs onto excitatory dendritic field A of the LGMD neuron, we designed a custom microscope allowing delivery of single-facet (ommatidium) stimuli onto the compound eye, while simultaneously imaging calcium signals generated by synaptic inputs onto field A (Fig. 1*A*). The location of the stimulus on the compound eye was registered by means of a CMOS camera that allowed simultaneous visualization of the stimulus and the compound eye (Fig. 1*B*). The excitatory dendrite of the LGMD was stained with OGB1, and, in conjunction with a custom-built upright two-photon microscope, the setup allowed us to acquire high-resolution images of field A (Fig. 1*C*).

Spatial distribution of calcium responses to single-facet stimuli. At the start of an experiment, a low-magnification image of dendritic field A was acquired and used to determine which dendritic branches were activated by the single-facet stimuli (Fig. 2*A*, *top*). This then allowed us to focus on specific dendritic segments receiving stimulus-activated synaptic inputs (Fig. 2*A*, *bottom*). In response to single-facet stimulation, we found that on average 4.2 distinct dendritic branches were activated (11 animals, 47 facets, standard deviation of 1.3 branches). On each branch the mean length of dendrite that exhibited significant relative changes in fluorescence was equal to 17 μm (standard deviation of 7.9 μm, 11 animals, 161 dendritic branches; Fig. 2*B*). By segmenting each branch in 2-μm-wide strips (Fig. 2*A*, *bottom*) and computing the average relative fluorescence change within each sequential strip, we obtained the spatial distribution of the relative fluorescence change, dF/F, and its evolution with time (Fig. 2*C*). We observed that the peak amplitude of dF/F on some branches was much stronger than on others (Fig. 2*C*). In addition, different locations on the same branch could exhibit large differences in the amplitudes of dF/F (Fig. 2*D*). On average, for each studied branch the peak dF/F was equal to 28.1% (standard deviation of 15.4%, 11 animals, 161 dendritic branches; Fig. 2*B*, *inset*). The average length of dendrite over which we observed calcium fluorescence changes was much larger than what is typically observed when single synaptic inputs are activated on dendrites (Goldberg et al. 2003). To investigate whether the differences in relative fluorescence seen at different locations and times along a single dendritic branch may be due to diffusion of calcium from a single entry point along the branch, we scrutinized the shape of the dF/F signal along each branch. As illustrated in one example in Fig. 2*E*, we detected little or no change over time in the shape of the spatial dF/F distribution after normalizing each curve to its peak value. This is in contrast to what would be expected from diffusion of calcium over the same distance (Helmchen and Nägerl 2016). Similar results were observed in 35 branches of 12 animals. This suggests that spatial differences in dF/F are not primarily due to calcium diffusion from a pointlike source. Thus a more likely explanation is that each dendritic segment receives multiple distinct synaptic inputs activated by the same facet that have different weights and that the location that generated the strongest responses received stronger synaptic input than adjacent locations. The locations of the synaptic inputs activated by a single facet within the excitatory dendritic field and their electrotonic distance are expected to have an impact on their integration, particularly for wide-field visual stimuli such as looming stimuli to which the LGMD is most sensitive. To quantify this aspect of the visual mapping, we computed the shortest dendritic distance between each pair of dendritic branches activated by a single-facet stimulus (Fig. 2*F*). By comparing this distribution with the shortest dendritic distances between spatially nearest pairs of tips (Fig. 2*F*, *top left inset*, black histogram) and with the shortest dendritic distances between any random pairs of tips (Fig. 2*F*, *top left inset*, blue histogram), we found that most of these activated branches had substantial dendritic separations. These large dendritic separations were observed despite the fact that the activated dendritic branches were spatially close to each other (Fig. 2*F*, *top right inset*, black histogram), and in particular

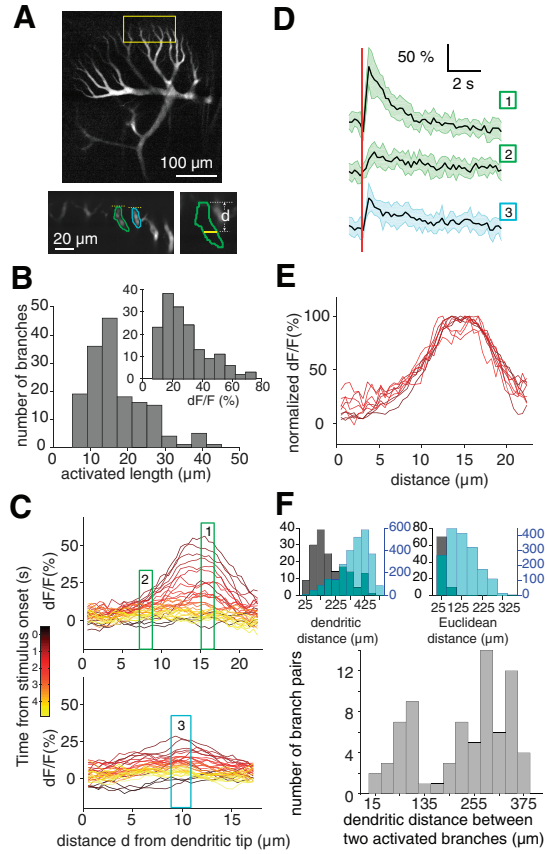

Fig. 2. Calcium responses in the LGMD's excitatory dendrite elicited by single-facet stimuli. *A*, *top*: image of an OGB1-filled LGMD neuron. The yellow rectangle indicates the region that contains the dendritic branches generating calcium responses to single-facet stimuli (50-ms OFF flash). *Bottom left*: expanded view of the dendritic branches in the yellow rectangle that were selected for further analysis in *C*–*E* (outlined in green and blue). *Bottom right*: the average dF/F was computed in each successive 2-μm-wide strip (indicated by yellow line) starting from the distal tip of each dendritic branch. d denotes the distance from the center of each strip to the dendritic branch tip. *B*: histogram of activated length, defined as the length on a dendritic branch that exhibits significant dF/F, i.e., the peak dF/F at each pixel is larger than 180% of the maximum noise of dF/F. *Inset*: histogram of the peak dF/F, computed as the peak of the average dF/F in the activated region on a dendritic branch (11 animals, 161 dendritic branches). *C*: spatial distribution of the average dF/F in each successive 2-μm-wide strip along the branches outlined in green and blue, respectively, in *A*. Different colors represent different times after the onset of the stimulus. The time courses of dF/F within the green and cyan rectangles are illustrated in *D*. *D*: time course of the average dF/F within the green rectangles (*1* and *2*) and within the cyan rectangle (*3*) in *C*. Black curve, mean of 10 trials; cyan and green shading, standard deviation. Red vertical line denotes the flash stimulus of 50-ms duration. *E*: normalized spatial distribution of the average dF/F in each successive 2-μm-wide strip along the branches outlined in green in *A*. Each trace is normalized to the peak. The darkest red trace and the lightest red trace are at 0.4 s and 1.7 s after the onset of the stimuli, respectively. Results similar to those presented in *A*–*D* were obtained in 5 other animals. *F*: histogram of the dendritic distances between 2 activated dendritic branches in response to single facet stimuli. The dendritic distance between the centers of every pair of activated branches was computed as the shortest dendritic path that connects them (6 animals, 14 single-facet stimuli, 74 activated dendritic pairs). *Top left inset*: black histogram shows the distribution of the shortest dendritic distances between every dendritic tip and its spatially nearest neighbor (i.e., having the shortest Euclidean distance; 6 animals, 167 pairs). Blue histogram shows the distribution of the shortest dendritic distances between any random pair of dendritic tips (6 animals, 2,669 pairs). *Top right inset*: black histogram shows the distribution of the Euclidean distances between activated dendritic branches in response to single-facet stimuli (6 animals, 74 pairs). Blue histogram shows the distribution of the Euclidean distances between any random pair of tips (6 animals, 2,669 pairs).

much closer than randomly selected dendritic tips (Fig. 2*F*, *top right inset*, blue histogram).

Preservation of fine retinotopy in the excitatory dendrite. Next, we studied the spatial pattern of synaptic activation generated by visual stimuli delivered at adjacent facets. Animals were presented with three single-facet stimuli along either the anterior-posterior axis or the dorsal-ventral axis (Fig. 3, *A* and *B*). As reported above, one facet activated more than one dendritic branch. In addition, we found that adjacent facets activated an overlapped portion of the same dendritic branches. We computed for each facet the COM of the activated dendritic branches and plotted its location along with the activated dendritic regions, as illustrated in Fig. 3, *C* and *D*. Because the dendritic regions activated by a single facet were typically discontinuous, the COM often fell between two adjacent dendritic branches. When we plotted the COMs associated with three successive facets stimulated along the posterior-anterior axis, we found that they were mapped in the same order along the medial-lateral axis of the LGMD dendrite (Fig. 3*E*). Similarly, facets stimulated along the dorsal-ventral axis were mapped to the dorsal-ventral dendritic axis (Fig. 3*F*). Thus the dendritic regions activated by different facets preserved retinotopy. As the distances between two stimuli increased from one facet to two and four facets, the distances between COMs also increased linearly along both directions of stimulation (Fig. 3, *G* and *H*; 1-facet distance along DV axis: $n = 6$ animals, fp = 11 facet pairs; AP axis: $n = 4$, fp = 15; 2-facet distance along DV axis: $n = 3$, fp = 6; AP axis: $n = 9$, fp = 12; 4-facet distance along DV axis: $n = 3$, fp = 3; AP axis: $n = 3$, fp = 3). The distance increased more steeply when the two stimuli were separated along the dorsal-ventral axis than along the anterior-posterior axis. In part, this was due to the fact that dendritic field A of the LGMD does not lie in a plane; instead, it curves more along the medial-lateral axis than along the dorsal-ventral axis. However, the distance between COMs was computed by projecting them onto the same z plane, which likely underestimated the real distances along the dorsal-ventral axis. To quantify the overlap between the dendritic regions activated on a single branch, we defined the overlap ratio as the ratio of the count of suprathreshold pixels that were activated by both stimuli and the count of the average suprathreshold pixels that were activated by the two individual stimuli. Pixels were deemed suprathreshold when the peak dF/F was >180% of the maximum noise of dF/F (see MATERIALS AND METHODS). As illustrated in Fig. 3, *I* and *J*, the overlap ratio between the dendritic branches activated by single-facet stimuli decreased as the separation of facets increased. There was almost no overlap when the separation was larger than four facets.

Adjacent facet inputs sum sublinearly and likely make independent synapses on the excitatory dendrite. When stimulating two facets simultaneously, will the elicited response be the sum of responses to the two individual stimuli? To address this question, we carried out imaging experiments in which we activated each of two facets either individually or simultaneously (Fig. 4*A*, left 3 columns). A comparison of the responses

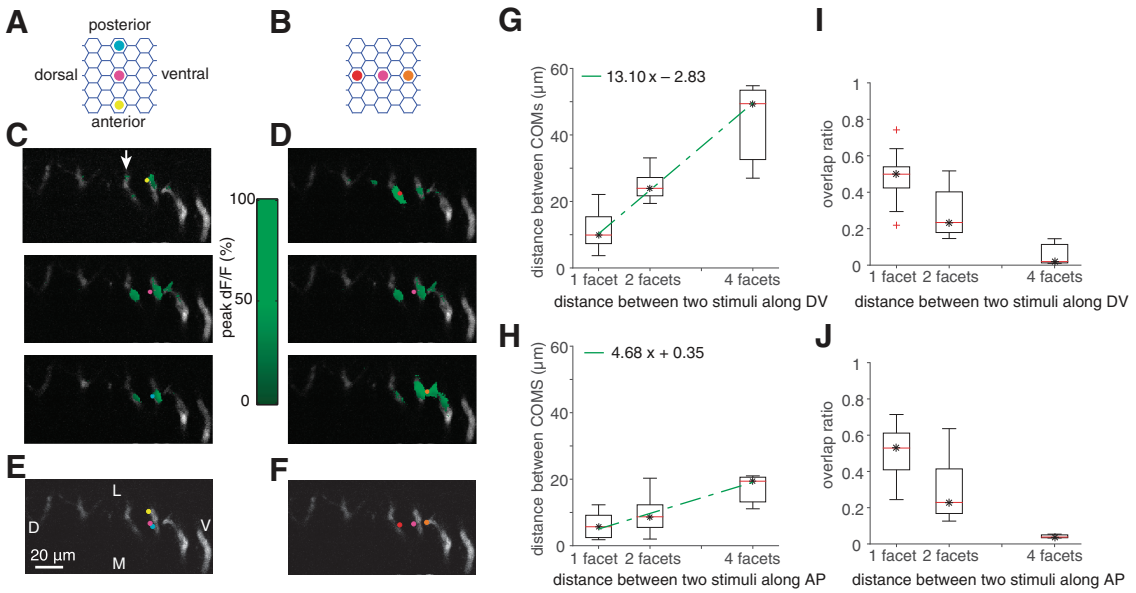

Fig. 3. Local structure of the retinotopic map on the LGMD excitatory dendrites. *A*: drawing illustrating the relative position of 3 single-facet stimuli along the anterior-posterior (A-P) eye axis (each stimulus is a 50-ms OFF flash). *B*: similar schematics of 3 single-facet stimuli along the dorsal-ventral (D-V) axis (50-ms OFF flashes). *C*: each panel illustrates the response to a single-facet stimulus along the A-P axis. From *top* to *bottom*: anterior, medial, and posterior stimuli, as illustrated in *A*. The intensity of green shading indicates for each pixel the peak dF/F amplitude at the corresponding dendritic location. In *top* panel, note the slight activation of the branch immediately to the left of the dendritic branch with the strongest response (arrow). The small round spots, color-coded as the stimuli in *A*, represent the centers of mass (COMs) of the peak dF/F across all pixels. *D*: peak dF/F in response to 3 single-facet stimuli along the D-V axis as illustrated in *B*. Same plotting conventions as in *C*. *E*: COM of peak dF/F responses for the 3 individual single-facet stimuli along the A-P axis, replotted from *C*. D, dorsal; V, ventral; M, medial; L, lateral. *F*: COM of peak dF/F responses for the 3 individual single-facet stimuli along the D-V axis, replotted from *D*. *G* and *H*: distances between COMs for 2 single-facet stimuli separated by 1 facet, 2 facets, or 4 facets along the D-V axis and the A-P axis, respectively. Green dashed lines and equations are linear fits to the 3 median values. *I* and *J*: overlap ratio of regions activated by 2 stimuli separated by 1 facet, 2 facets, or 4 facets along the D-V axis and the A-P axis, respectively. Optimal linear fits for distances ranging from 1 to 4 facets given by: $y = -0.15x + 0.61$ and $y = -0.15x + 0.62$, respectively. In *G*–*J* red lines are the median of the data; the bottom and the top of each box are the first and the third quartiles. The whiskers represent the extent of the data (1-facet distance along D-V axis: $n = 6$ animals, fp = 11 facet pairs; A-P axis: $n = 4$, fp = 15; 2-facet distance along D-V axis: $n = 3$, fp = 6; A-P axis: $n = 9$, fp = 12; 4-facet distance along D-V axis: $n = 3$, fp = 3; A-P axis: $n = 3$, fp = 3).

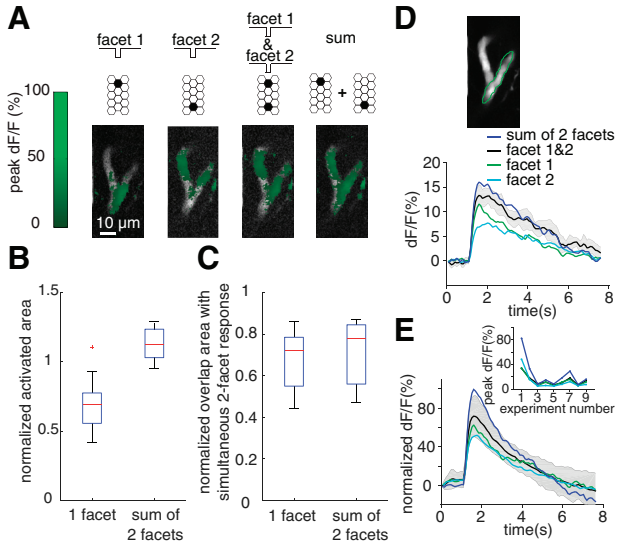

Fig. 4. Calcium responses to simultaneous stimuli are approximately the sum of responses to 2 single-facet stimuli. *A*: from *left* to *right*, responses to different single-facet stimuli (*facets 1* and *2*) along the anterior-posterior axis (*top insets*); response to 2 simultaneous single-facet stimuli; and sum of single facet responses corresponding to *facets 1* and *2*. *B*, *left*: size of area activated by 1 facet normalized to simultaneous 2-facet response area. *Right*: sum of the area size activated by 2 single-facet stimuli normalized to simultaneous 2-facet response area. *C*, *left*: overlap ratio of activated regions between single-facet response and simultaneous 2-facet response. *Right*: overlap ratio of activated regions between the sum of responses to 2 single-facet stimuli and simultaneous 2-facet response. In *B* and *C*, red lines are the median of the data; the bottom and the top of the box are the first and the third quartiles. The signed-rank tests reported in the text were performed on 13 single-facet stimuli and 9 pairs of simultaneous 2-facet stimuli in 4 animals. *D*, *top*: a selected portion of the dendritic branch outlined in green is analyzed. *Bottom*: time courses of the average dF/F within the green outlined area in response to single-facet stimuli, to a simultaneous 2-facet stimulus, or to the sum of responses to 2 single-facet stimuli. Gray shading: standard deviation of 5 trials. *E*: average dF/F of 9 pairs of facets in 4 animals (normalized to peak dF/F of sum of responses to 2 single-facet stimuli) in response to single-facet stimuli, to a simultaneous 2-facet stimulus, or to the sum of responses to 2 single-facet stimuli. Gray shading: standard deviation of 9 experiments. *Inset*: original peak dF/F across experiments (9 pair of stimuli in 4 animals).

to the two simultaneous stimuli and the summed response to two individual facets revealed similar activation patterns (compare right 2 columns in Fig. 4*A*).

To quantify the relationship between the responses to simultaneous and summed stimuli, while taking into account the fluctuations of fluorescence signals across branches and preparations, we first computed the activated area by counting the suprathreshold pixels in response to individual facet stimuli. For illustration purposes, the activated area of a single-facet stimulus or the summed responses to two individual stimuli was then normalized to the activated area in response to the two simultaneous stimuli (Fig. 4*B*). We found that the normalized activated area in response to individual facet stimuli was 0.69, ~40% more than half the area activated by two simultaneously stimulated facets. Accordingly, the area activated by one facet was significantly larger than half the area activated by two facets ($P = 0.0007$, signed-rank test; see MATERIALS AND METHODS). The normalized area activated by the summed response of individual facets was 1.13; the summed response area was again significantly larger than that activated simultaneously by two facets ($P = 0.02$, signed-rank test). These results imply that the area activated by two simultaneously activated facets is smaller than what would be expected from a simple addition of individual responses. Next, we computed the overlap between the region activated by an individual facet and the region activated by two simultaneous stimuli (computed as in Fig. 3, *G* and *H*). The overlap area was normalized by the area activated by a single facet and was equal to 0.72 (Fig. 4*C*). The difference in these two areas was significant ($P = 0.0001$, signed-rank test). In addition, we computed the overlap between the region activated by summed responses and the region activated by two simultaneous stimuli. The overlap area was normalized by the area activated by two simultaneous stimuli. The normalized overlap ratio of these two areas was 0.78 (Fig. 4*C*), and the difference in areas was again significant ($P = 0.004$, signed-rank test). These results suggest that, when stimulated alone, single facets activate areas outside the area activated by both facets simultaneously.

The time course of the average dF/F on a selected dendritic branch (Fig. 4*D*, *top*) also revealed that the peak dF/F in response to two simultaneous stimuli was slightly, but not significantly, smaller than that of the summed response to two individual stimuli. By normalizing the dF/F to the peak dF/F of the summed response, we computed the average of the normalized dF/F across nine pairs of stimuli in four animals (Fig. 4*E*; original peak dF/F values are shown in *inset*). The response to two simultaneous stimuli was larger than the response to individual stimuli while remaining slightly, but not significantly, smaller than the summed response to the two individual stimuli. Similar results were obtained when we repeated this analysis restricted to the common area activated by each individual facet and simultaneously by both facets (not shown).

As noted above, stimulating adjacent facets activated a common portion of a branch on the excitatory dendrite (Fig. 5*A*). Do adjacent facets that elicit a response in the same dendritic branch make independent synapses, or do they share common synapses over the dendritic region they activate? To address this question, we took advantage of the fact that the excitatory inputs activated on dendritic field A by small visual stimuli (5°) strongly habituate in response to repeated stimulation and this habituation is most likely to be located at the presynaptic terminal of the LGMD (O'Shea and Rowell 1976). Hence, if we stimulate the same synaptic input in rapid succession, we expect the second stimulation to elicit a weaker calcium response. If two facets share common synaptic input we would thus expect the activation of the second facet to result in weaker calcium signals after activation of the first one. Conversely, if the two facets do not share synaptic inputs, then activation of the second facet should not depend on the prior activation of another facet. In the following experiments, we thus focused on dendritic branches activated by two adjacent facets, as illustrated in Fig. 5*A*. We stimulated each facet twice with an interval of 0.2 s between stimuli (Fig. 5, *B* and *C*) and compared the responses to those elicited by stimulation of either facet followed by the other one (Fig. 5, *D* and *E*). The same experiment was repeated with a 1-s-long interstimulus interval for which habituation will be minimized (Fig. 5, *F–I*). Additionally, we used an intermediate interval of 0.5 s. We compared the response to the second pulse (P2) with the first pulse (P1, Fig. 5*I*) by computing a paired-pulse peak response ratio P2/P1 (Fig. 5*J*). By comparing the responses to sequential stimulation of the same facet, we found that paired-pulse ratios increased with the interstimulus interval, as expected from

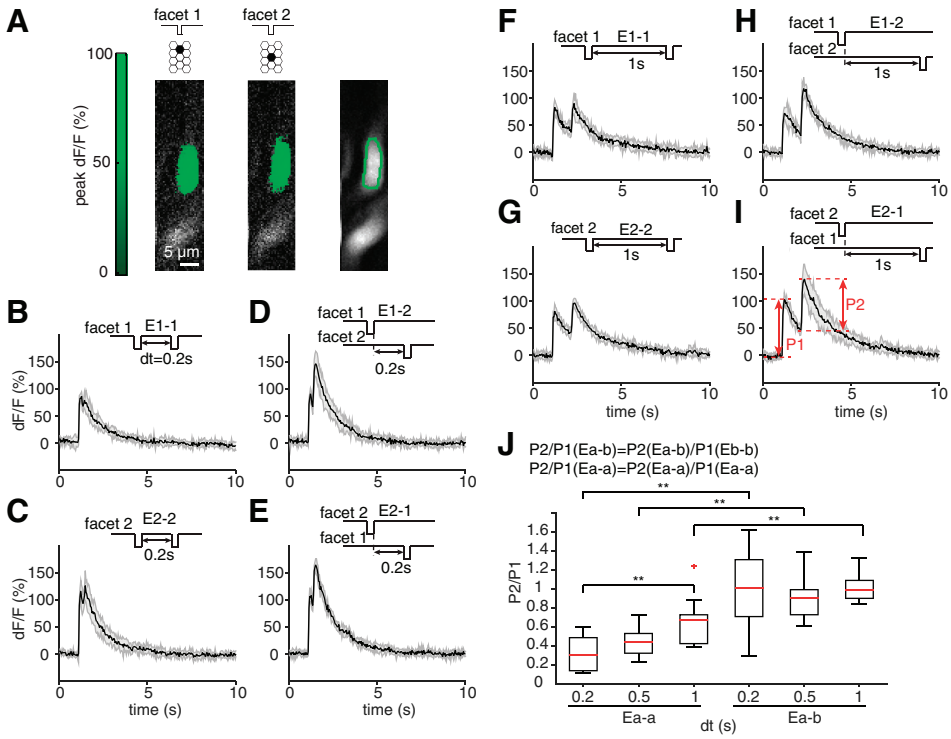

Fig. 5. Calcium signals are consistent with different facets making independent synapses onto the same dendritic branch. *A*, *left*: the peak dF/F (averaged over 5 trials) in a dendritic branch activated by *facet 1*. *Center*: the peak dF/F (averaged over 5 trials) in the same dendritic branch activated by *facet 2*. *Right*: the region selected to compute the average dF/F in *B–I*. *B* and *C*: responses to 2 single-facet stimuli separated by a time interval of 0.2 s at 2 adjacent *facets 1* and *2*, respectively. *D* and *E*: sequential stimulation at *facet 1* followed by *facet 2* (*D*) or at *facet 2* followed by *facet 1* (*E*) with an interval of 0.2 s. *F* and *G*: responses to 2 single-facet stimuli separated by a time interval of 1 s at 2 adjacent *facets 1* and 2, respectively. *H* and *I*: sequential stimulation at *facet 1* followed by *facet 2* (*H*) or at *facet 2* followed by *facet 1* (*I*) with an interval of 1 s. In *I*, the amplitudes of the 1st and 2nd peaks are marked in red as P1 and P2. In *B–I*, the time courses of average dF/F are taken from the portion of the dendritic branch outlined in green in *A*. *Insets* are stimulation protocols. Black curves are means of 5 trials; gray shades are standard deviations of 5 trials. *J*: the ratio of the 2nd peak to the 1st peak either in the protocol using 2 different stimuli (Ea-b) or twice the same stimuli (Ea-a) with 3 different time intervals (d*t*) of 0.2 s, 0.5 s, and 1 s. **Significant difference at the $P < 0.005$ level (Mann-Whitney *U*-test; 10 Ea-a and 16 Ea-b stimulated facets and recording locations in $n = 4$ animals).

habituation of synaptic responses (Fig. 5*H*, Ea-a). In contrast, paired-pulse ratios of the two-facet stimulation protocol (Ea-b) were significantly higher at all three intervals of 0.2, 0.5, and 1 s (10 Ea-a and 16 Ea-b in 4 animals). In addition, the paired-pulse ratios did not increase with increasing interstimulus interval. Taken together, these results suggest that synaptic inputs originating from different facets are independent of each other.

Calcium and membrane potential responses to local translational stimuli. Given that adjacent facets provide independent synaptic inputs to common portions of dendrites, we wondered how this wiring diagram might influence the response of the cell to local translational stimuli. We designed a simple stimulus protocol that covered three adjacent facets along the dorsal-ventral axis and identified the three dendritic compartments most strongly activated by these stimuli (Fig. 6*A*). As illustrated in Fig. 6*B*, *top*, the protocol consisted of three OFF steps activated in sequence with a time interval of 0.4 s between the activation of two facets in two directions, ventral to dorsal and dorsal to ventral (Fig. 6*B*, *top left* and *top right*, respectively). We recorded the LGMD membrane potential with an intracellular electrode inserted in the main trunk of the excitatory dendritic field (Fig. 6*B*, *bottom*). Simultaneously, we recorded the calcium signals in the three dendritic compartments (Fig. 6*C*, black traces; 1 row per dendritic compartment). The membrane potential responses were considerably faster than the associated calcium traces at the location of maximal synaptic activation. We saw no directional selectivity in the membrane potential recorded in the main trunk of the dendrite, far from the region where calcium signals were recorded ($n = 3$ animals). In contrast, the more dorsal and ventral dendritic compartments showed asymmetric responses to the two directions of motion (Fig. 6*C*, *top* and *bottom*), while the middle compartment did not (Fig. 6*C*, *middle*). To explain these local differences, we recorded the calcium responses to single 50-ms OFF flashes presented at the same three facets. The single-facet responses on different branches preserved retinotopy (Fig. 6, *D–F*) so that the middle branch was activated almost equally by the three facets (Fig. 6*E*), while the branch more dorsal or ventral received stronger synaptic inputs from the facet more dorsal or ventral, respectively (Fig. 6, *D* and *F*). We found that the calcium responses to the translational stimuli were approximately fit by the linear sum of the three single-facet flash responses delayed by 0.4 s between two adjacent responses (Fig. 6*F*, red traces; similar results were obtained in 4 animals). Since the synaptic inputs on the branch at the center were equally weighted from the three facets, the response to the translational stimuli in the two directions had similar shapes. The unevenly weighted synaptic inputs on the dorsal and ventral branches caused dissimilar shapes of dF/F in the two different moving directions.

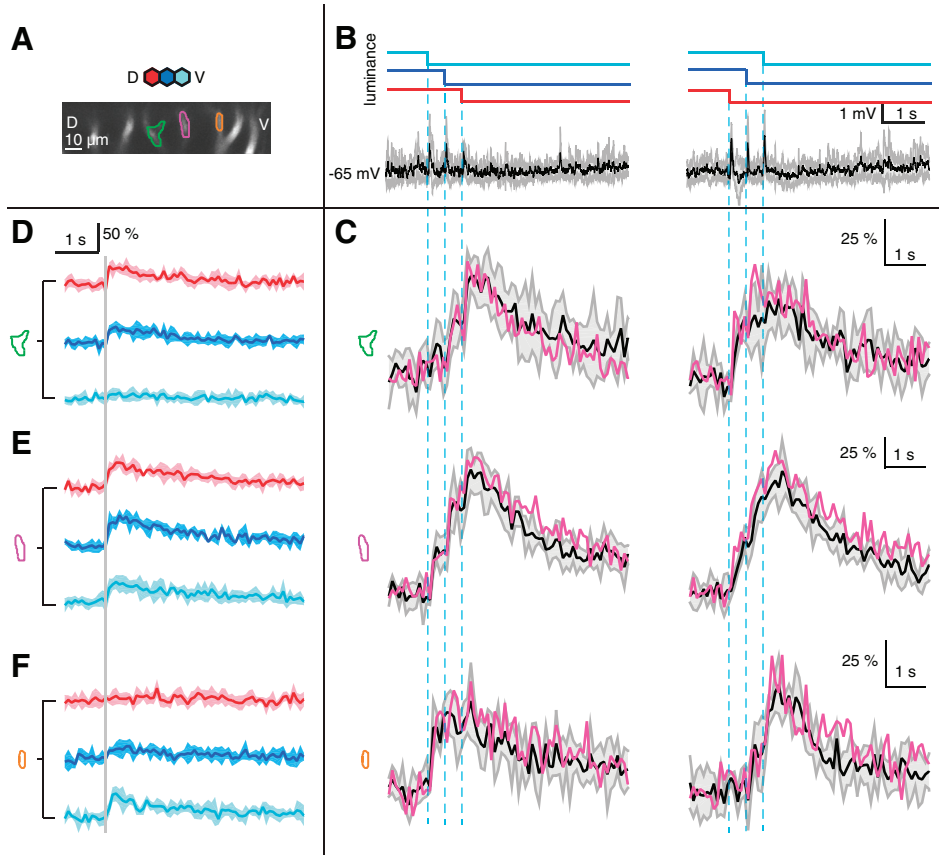

Fig. 6. Calcium responses to translating single-facet stimuli along the dorsal-ventral axis. *A*, *top*: schematic illustration of 3 adjacent facets along the dorsal-ventral (D-V) axis. Each facet is color coded from *left* to *right* in red, blue, and cyan, respectively. The same color code is used for stimulation traces in *B* and for relative fluorescence traces in *D–F*. *Bottom*: illustration of the dendritic branches in green, magenta, and orange selected for analysis in *C–F*. *B*, *top*: the stimulation protocols. Three adjacent facets are stimulated by OFF luminance steps separated by 0.4 s. *Bottom*: intracellular recording from the main trunk of the LGMD excitatory dendrite. Spikes were removed by applying a median filter over a time window of 8 ms. A notch filter has been applied to remove 60 Hz noise. Black trace is the average of 3 animals, 3–5 trials per animal. *C*: relative fluorescence change in response to the protocols depicted in *B*. Black traces are the relative fluorescence change in response to the sequential stimulation of 3 facets along the dorsal-ventral axis in the direction of V to D (*left*) and D to V (*right*) with a 0.4-s time interval between 2 adjacent stimuli, respectively. Gray shading is the standard deviation of 5 trials. Pink traces are the linear summation of the single facet responses illustrated in *D–F* with a 0.4-s time delay between 2 adjacent responses. *D–F*: relative fluorescence change in response to the 3 single-facet stimuli represented in red, blue, and cyan. Gray vertical line denotes the 50-ms OFF flash stimuli.

For translational stimuli covering three facets along the anterior-posterior axis (Fig. 7*A*), we again observed little directional selectivity of the membrane potential recorded in the main dendritic trunk (Fig. 7*B*; $n = 3$ animals). The lateral dendritic compartment outlined in green in Fig. 7*A* exhibited little dependence of calcium responses to movement direction (Fig. 7*C*, *top*), while the medial dendritic compartment showed more pronounced differences (Fig. 7*C*, *bottom*). We analyzed again responses to 50-ms OFF flashes at both locations (Fig. 7, *D* and *E*) and found that the larger differences seen at the medial location correlated well with the differences seen in response to translating stimuli. Additionally, the portion of dendritic branches located laterally received stronger synaptic inputs from the anterior facets compared with the medial branch, as predicted by the retinotopic mapping. As for dorsal-ventral stimuli, the responses to translational stimuli in the direction of posterior to anterior and anterior to posterior were approximately equal to the linear sum of the single-facet responses, with 0.4 s between two adjacent responses (Fig. 7*C*, red traces; similar results were obtained in 4 animals). Therefore, knowing single-facet flash responses allowed us to predict the shape of the calcium responses to local translational stimuli.

Calcium and membrane potential responses to dynamic visual stimuli. The LGMD neuron is most sensitive to looming stimuli, simulating objects approaching on a collision course toward the animal (Hatsopoulos et al. 1995; Rind and Simmons 1992; Schlotterer 1977). At the level of individual facets, these stimuli may be approximated by dark edges translating across the receptive field of their associated photoreceptors (Jones and Gabbiani 2010). The translation speed increases the closer facet activation is to collision time (Gabbiani et al. 1999). The spatial receptive field of a locust photoreceptor can be modeled as a circularly symmetric Gaussian function (Jones and Gabbiani 2010). Hence, when a dark edge moves across such a receptive field at a constant angular speed, the time course of luminance change at the photoreceptor will have the shape of a cumulative Gaussian. We therefore employed single-facet stimuli with a luminance time course given by a cumulative Gaussian to simulate the signals expected to impinge on a photoreceptor when stimulated by an edge translating at constant speed (Fig. 8*A*, *top*; Jones and Gabbiani 2010). Each stimulus was characterized by its luminance change duration, defined as 6 times the standard deviation of the temporal Gaussian used to compute the cumulative profile of luminance decrease. Accordingly, the four stimuli had luminance change durations of 0, 57, 110, and 226 ms, corresponding, respectively, to an instantaneous flash and to translating velocities of 0.4 mm/s, 0.2 mm/s, and 0.1 mm/s, based on the average size of a facet (24 μm). In agreement with earlier results, the amplitude of the LGMD membrane potential depolarization was stronger when the luminance change duration was shorter (Fig. 8*A*, *middle*; Jones and Gabbiani 2010). Plotted on the same timescale, calcium responses were on average much slower (Fig. 8*A*, *bottom*). Inspection of the entire dF/F response time course revealed an increase in peak response with decreasing luminance change duration that paralleled the result seen for peak membrane potential (Fig. 8*B*). When we plotted peak dF/F as a function of peak membrane potential, we found a relation close to linear between the two variables (Fig. 8*C*; 3 facets in 1 animal). A similar dependence of peak LGMD membrane potential depolarization and peak dF/F as a function

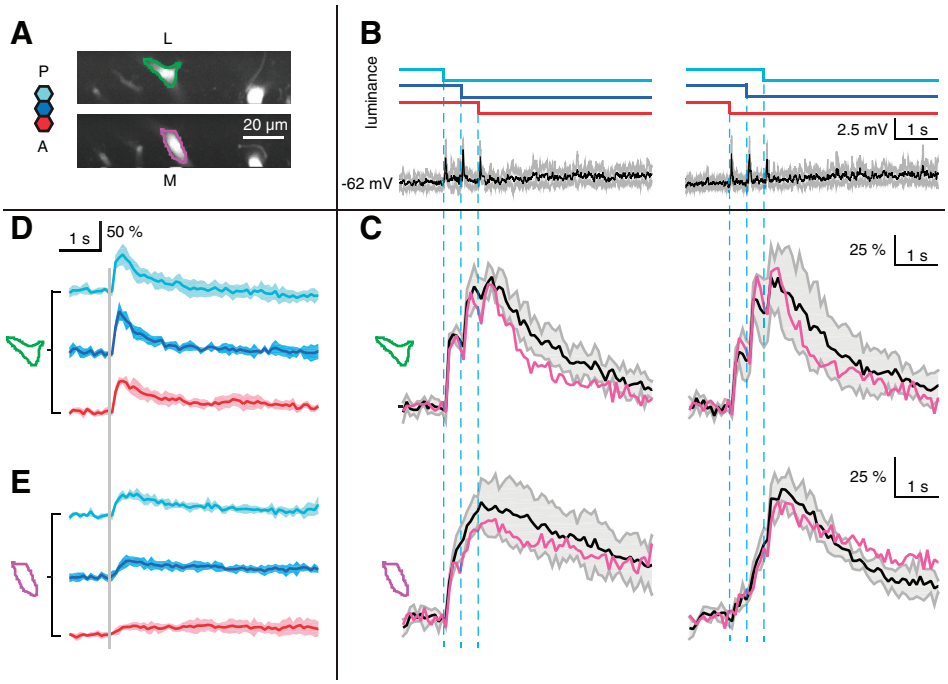

Fig. 7. Calcium responses to translating single-facet stimuli along the posterior-anterior axis. *A*, *left*: schematic illustration of 3 adjacent facets along the posterior-anterior (P-A) axis. *Right*: images of the same dendritic area in 2 different *z*-planes separated by 7 μm and activated by the stimuli. *Top*: a thinner branch is in focus. *Bottom*: a thicker branch is in focus. Green and magenta outline the portions of dendritic branches selected for analysis in *D* and *E*, respectively. L, lateral; M, medial. *B*, *top*: stimulation protocols. Three adjacent facets are stimulated by OFF steps with 0.4 s between 2 successive steps in the direction of P to A (*left*) and A to P (*right*), respectively. *Bottom*: intracellular recording from the LGMD excitatory dendrite. Spikes were removed by applying a median filter with a time window of 8 ms. A notch filter has been applied to remove 60-Hz noise. Black trace is the average of 3 animals, 3–5 trials per animal. *C*: black traces are the relative fluorescence change in response to the sequential stimulation depicted in *B* of 3 facets along the P-A axis: data acquired at the lateral location (*top*) and at the medial location (*bottom*). Gray shading is the standard deviation of 5 trials. Red traces are the linear sum of the single-facet responses in *D* and *E* with 0.4-s time delay between 2 successive responses. *D* and *E*: relative fluorescence change in response to the 3 single facet stimuli represented in cyan, blue, and red. Gray vertical line denotes the 50-ms OFF flash stimuli.

of luminance change duration was observed in eight different facets across four animals, although there was variability in both the maximal response and the slope of the relation between experiments (Fig. 8*D*). The pooled dependence of peak dF/F on peak membrane potential depolarization was again close to linear (Fig. 8*E*). Linear fits carried out in each individual experiment revealed a range of slopes, whose median was close to the slope obtained across the pooled data set (Fig. 8*E*, *inset*).

Next, to mimic on a microscopic scale the typical looming stimulation patterns to which the LGMD is most sensitive, we delivered expanding black stimuli that covered three concentric layers of facets (Fig. 8*F*) with different expansion durations of 0 (instantaneous), 0.6, and 1.3 s. The slope of the rising edge of the calcium responses followed closely the slopes of the expanding stimuli (Fig. 8*G*; $n = 3$ animals). Based on the assumption of linear summation and the overlap ratios of the activation patterns between adjacent facets obtained in Fig. 3, *I* and *J* (see MATERIALS AND METHODS), we modeled the calcium responses to different expansion speeds (Fig. 8*G*, *bottom inset*, dotted lines) and found that they fitted well with the experimental data.

DISCUSSION

The results presented here directly demonstrate that the LGMD receives a distributed, fine retinotopic projection from the locust compound eye. In response to single-facet stimuli, synaptic inputs are activated on branches that have large dendritic separations, yet the COM of those activated branches preserves retinotopy at the finest possible level. We also discovered that adjacent facets activate an overlapping portion of the same dendritic branches. In addition, we demonstrated that adjacent facets most likely make independent synapses on the excitatory dendrite of the LGMD. We established that in response to local translational stimuli the calcium responses could be approximated by the linear sum of the single-facet calcium responses and that they revealed dendritic activation patterns inaccessible to intracellular recordings. We also found that the amplitude of the peak membrane potential is linearly related to the peak dF/F in response to single-facet stimuli with different rates of luminance change. Finally, we demonstrated that the slopes of the rising edge of the relative fluorescence change dF/F increases as the rate of local stimulus expansion increases.

Because of the buffering properties of calcium indicators, relative calcium fluorescence signals can only be an indirect indicator of the local membrane potential (Yaksi and Friedrith 2006). In the LGMD, dendritic calcium signals are entirely due to calcium entry through nicotinic acetylcholine receptors because the dendritic fields of the LGMD are devoid of voltage-gated calcium channels (Peron and Gabbiani 2009). Thus the results reported here can be directly linked to synaptic activation. The amplitude of the peak relative fluorescence signal dF/F depends on the concentration of the calcium indicator (Helmchen et al. 1996). Thus differences in the amount of calcium indicator injected into neurons of different animals can lead to different amplitudes of the peak dF/F. In general, the

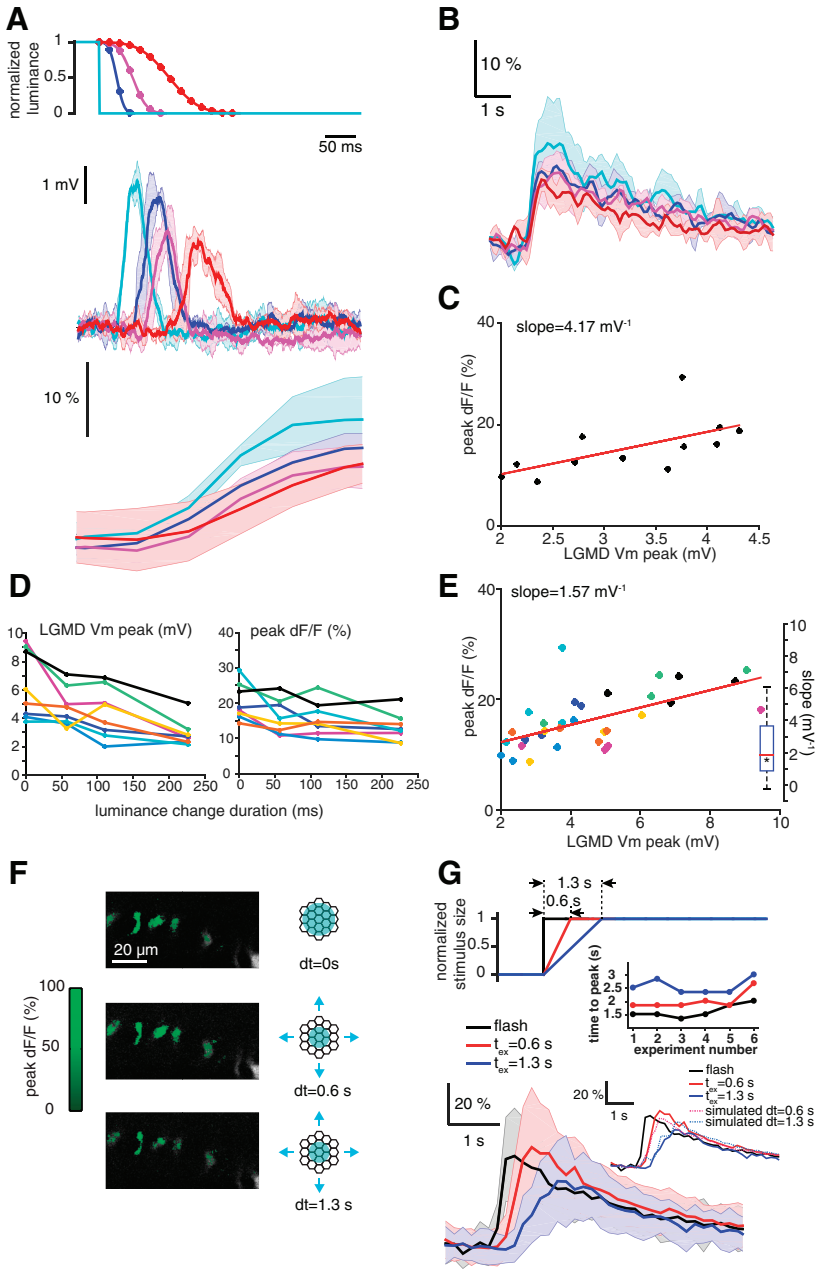

Fig. 8. Calcium responses to different speeds of stimulus change. *A*, *top*: single-facet stimuli with different rates of luminance change that simulate a dark object moving across the Gaussian-shaped receptive field of a single photoreceptor with different translational speeds. *Middle*: corresponding LGMD membrane potential responses. *Bottom*: dF/F of selected dendritic branches on the LGMD. Each trace is averaged from the responses of 3 facets in 1 animal (5 trials/facet). *B*: zoomed-out view of the dF/F changes depicted in *A*. *C*: peak dF/F as a function of peak membrane potential (V_m) in LGMD intracellular recordings (3 facets in 1 animal). Red line is linear fit to the data ($R^2 = 0.37$, $P = 0.035$). *D*, *left*: relation between peak LGMD V_m and luminance change duration. *Right*: relation between peak dF/F and luminance change duration (8 facets in 4 animals; each experimental data set is plotted in a different color). *E*: peak dF/F as a function of peak LGMD V_m pooled across experiments. Different colors represent different stimulus locations or animals (matched with colors in *D*). Red line is the linear fit of all the data points (8 facets in 4 animals, $R^2 = 0.38$, $P = 0.0002$). *Inset*: box plot of the slopes calculated from linear fits to each individual experiment. Red line is the median of the data; the bottom and the top of the box are the first and the third quartiles; the star is the slope obtained from the pooled data in the main panel. *F*: calcium responses to an OFF flash stimulus that covers 3 concentric facet layers (*top*) and to concentrically expanding stimuli with an expansion duration of 0.6 s and 1.3 s (*middle* and *bottom*). The stimulation protocols for flash stimuli and expansion stimuli are shown on *right*. Peak dF/F (averaged over 5 trials) in dendritic branches activated by the 3 different stimuli is illustrated on *left*. *G*: average dF/F of selected dendritic branches in 3 animals in response to 3 stimulus expansion durations, flash (black), $t_{ex} = 0.6$ s (red), and $t_{ex} = 1.3$ s (blue). Normalized stimulus sizes as functions of time are shown at *top*. *Top inset*: time of the peak dF/F across different animals (6 dendritic branches in 3 animals). *Bottom inset*: comparison of the experimental data (thick lines) and the simulated data (dotted lines). In *A*, *B*, and *G* shaded areas represent the SD of each data set.

diffusion of the calcium indicator within the neuron will depend on the location of the blindly selected dye injection site and on the thickness of the branches, which can also lead to inhomogeneous concentrations across different branches. Therefore, the absolute value of the peak dF/F cannot be used to measure in a single neuron the amount of calcium influx at locations with high baseline fluorescence differences, or across different animals, but it can be used to compare the calcium responses in the same branch or a few branches with similar baseline fluorescence. However, we found consistent changes of the dF/F signal with stimulus parameters when stimulating different facets in the same animal and across animals. In particular, our experiments demonstrate that it is possible to compare the relative responses across different animals to visual stimuli with different rates of luminance change or different moving speeds.

Our results show that synaptic inputs from a single facet wire onto several spatially separated dendritic branches. Most of the activated branches have large dendritic separations, in contrast to assumptions in previous modeling work (Peron et al. 2007). We also found that activation of two adjacent single-facet inputs sum sublinearly, in agreement with our earlier results based on membrane potential recordings (Jones and Gabbiani 2010). In addition, the measured calcium responses strongly suggest that adjacent facets make independent synaptic inputs on the same portion of dendritic branches. Which anatomical wiring scheme between presynaptic afferents and dendrites in field A of the LGMD could explain these results? One possibility would be for each presynaptic afferent axon to branch into several terminals as it enters the lobula, with each terminal making several synaptic contacts along a given LGMD dendrite. This arrangement would be able to

explain our calcium imaging results if in addition the synapses of distinct afferents were intermingled on individual dendritic segments. Recent electron microscopic reconstructions suggest that this is indeed how presynaptic afferent terminals are anatomically organized in relation to LGMD dendrites (F. C. Rind, personal communication).

This independent but overlapping wiring scheme increases the effective "receptive field" of every dendritic branch and also prolongs the activation time of each branch when a stimulus moves across several adjacent facets compared with what would be expected from a nonoverlapped wiring scheme. These observations are particularly interesting in view of the fact that the excitatory dendritic field of the LGMD contains several active conductances, including a prominent I_h and voltage-activated potassium conductances (R. Dewell and F. Gabbiani, unpublished observations). We thus expect that in response to large visual stimuli that activate several dendritic branches such as looming stimuli, the distributed and overlapping wiring scheme will have an impact on the local activation of these conductances. In particular, the interaction between retinotopic synaptic inputs and active dendritic conductances could increase responses to looming stimuli and opposed to matched, spatially randomized controls, thus implementing a form of visual object segmentation (R. Dewell and F. Gabbiani, unpublished observations). Testing this hypothesis will require us to incorporate the wiring scheme and active conductances in detailed compartmental simulations of the LGMD neuron along the lines of our previous simulations (Jones and Gabbiani 2012).

The peak of the membrane potential of the LGMD recorded in thicker dendrites and the peak dF/F in smaller dendrites inaccessible to intracellular recordings exhibited a linear relationship. This relationship was evident both in individual and in pooled experiments, yet there was clearly variability across individual experiments, since the slopes of the linear fit spanned a wide range across the animals. One reason for this is that the membrane potential responses to single-facet stimuli can vary across animals depending on the state of each animal and details of the dissection process. Therefore, the median-filtered membrane potential depolarizations elicited by the stimuli could vary over a large range across animals. Another source of variability is that the calcium response to a single-facet stimulus with slow luminance change was relatively small, resulting in a modest signal-to-noise ratio.

The fast rising edge of dF/F in response to a local expanding stimulus captures its speed of expansion. In future experiments, it will be interesting to determine directly the membrane potential change in various dendritic branches in response to an expanding or a looming stimulus. This would require using genetically encoded voltage indicators or voltage-sensitive dyes, neither of which have yet proven technically feasible in the LGMD.

The previous study by Peron et al. (2009) showed directional selectivity of the peak firing rate and synaptic calcium responses of the LGMD for local motion using a $10° \times 10°$ stimulus moving at 40°/s over a wide portion of the visual field. Here we did not find similar directional selectivity of calcium responses and firing rate or median-filtered membrane potential over three sequential single-facet stimuli moving at the equivalent of 7.5, 15, or 30°/s. One explanation for this difference might be that observing directional selectivity requires activation of a larger number of facets, which would be difficult to produce under the stimulation configuration used in our experiments. These observations underscore the difficulty in extrapolating LGMD's responses from localized to extended visual stimuli. For example, when a looming stimulus is large and fast changing, it simultaneously activates many synaptic inputs expected to interact nonlinearly with active dendritic conductances. Exploring the significance of results such as those illustrated in Fig. 6 and Fig. 7 will thus require compartmental simulations incorporating dendritic voltage-activated conductances.

Two-photon imaging enables high spatial resolution and deep penetration depth compared with wide-field CCD imaging used to study the retinotopy of the LGMD previously (Peron et al. 2009). However, the higher spatial resolution also resulted in a restricted depth of focus, therefore requiring five to seven images at successive depths to obtain a complete image of one branch, particularly close to the lateral tips of the LGMD dendrites that exhibit high curvature. The shot noise of two-photon imaging is higher than that of CCD imaging because of the smaller amount of photons collected (Homma et al. 2009), which made it difficult to distinguish relative fluorescence signals from noise, particularly when the dF/F was $<10\%$. Despite this limitation, two-photon imaging was highly suitable to studying retinotopy at a fine resolution in vivo. In preliminary tests conducted with both CCD and two-photon imaging in the same preparation we could clearly demonstrate the substantially higher spatial resolution of two-photon imaging. To further improve the in vivo temporal and spatial resolution and enable simultaneous imaging of the whole dendrite in three dimensions, emerging techniques such as holographic imaging with a spatial light modulator (Nikolenko et al. 2008; Quirin et al. 2014) and lattice light sheet microscopy (Chen et al. 2014; Li et al. 2015) could be employed in future experiments.

Two-photon calcium imaging in conjunction with single-facet stimulation proved to be powerful tools to dissect the fine topographic mapping from the locust eye onto the excitatory dendrite of the LGMD as well as the dynamics of calcium signals in response to time-varying visual stimuli. In particular, they revealed the fine and distributed retinotopic mapping from single facets and the overlapped wiring scheme from adjacent facets. This detailed knowledge is necessary to accurately model the mechanisms of synaptic integration within the LGMD and better understand the dendritic computations carried out by this neuron. The techniques developed in this work also pave the way for future investigations of calcium and membrane potential signals in fine dendrites of the LGMD in response to looming stimuli.

ACKNOWLEDGMENTS

We thank Drs. P. Saggau and E. Froudarakis for technical assistance in building the two-photon microscope. We also thank Drs. R. Dewell and H. Wang for assistance with electrophysiological recording techniques and E. Sung for help with the neuron reconstructions.

GRANTS

This work was supported by grants from the National Science Foundation (DMS-1120952) and the National Institutes of Health (NIH) (MH-065339) as well as a National Eye Institute/NIH Core Grant for Vision Research (EY-002520-37).

DISCLOSURES

No conflicts of interest, financial or otherwise, are declared by the author(s).

AUTHOR CONTRIBUTIONS

Y.Z. and F.G. conception and design of research; Y.Z. performed experiments; Y.Z. analyzed data; Y.Z. and F.G. interpreted results of experiments; Y.Z. and F.G. prepared figures; Y.Z. and F.G. drafted manuscript; Y.Z. and F.G. edited and revised manuscript; Y.Z. and F.G. approved final version of manuscript.

REFERENCES

Adams DL, Horton JC. A precise retinotopic map of primate striate cortex generated from the representation of angioscotomas. *J Neurosci* 23: 3771–3789, 2003.

Bollmann JH, Engert F. Subcellular topography of visually driven dendritic activity in the vertebrate visual system. *Neuron* 61: 895–905, 2009.

Burrows M, Rowell CH. Connections between descending visual interneurons and metathoracic motoneurons in the locust. *J Comp Physiol* 85: 221–234, 1973.

Chen BC, Legant WR, Wang K, Shao L, Milkie DE, Davidson MW, Janetopoulos C, Wu XS, Hammer JA 3rd, Liu Z, English BP, Mimori-Kiyosue Y, Romero DP, Ritter AT, Lippincott-Schwartz J, Fritz-Laylin L, Mullins RD, Mitchell DM, Bembenek JN, Reymann AC, Böhme R, Grill SW, Wang JT, Seydoux G, Tulu US, Kiehart DP, Betzig E. Lattice light-sheet microscopy: imaging molecules to embryos at high spatiotemporal resolution. *Science* 346: 1257998, 2014.

Dewell RB, Gabbiani F. Linking dendritic processing to computation and behavior in invertebrates. In: *Dendrites* (3rd ed.), edited by Stuart G, Spruston N, Häuser M. Oxford, UK: Oxford Univ. Press, 2016.

Euler T, Detwiler PB, Denk W. Directionally selective calcium signals in dendrites of starburst amacrine cells. *Nature* 418: 845–852, 2002.

Fotowat H, Gabbiani F. Collision detection as a model for sensory-motor integration. *Annu Rev Neurosci* 34: 1–19, 2011.

Franceschini N, Kirschfeld K. Pseudopupil phenomena in the compound eye of *Drosophila*. *Kybernetik* 9: 159–182, 1971.

Gabbiani F, Krapp HG, Koch C, Laurent G. Multiplicative computation in a visual neuron sensitive to looming. *Nature* 420: 320–324, 2002.

Gabbiani F, Krapp HG, Laurent G. Computation of object approach by a wide-field, motion-sensitive neuron. *J Neurosci* 19: 1122–1141, 1999.

Gias C, Hewson-Stoate N, Jones M, Johnston D, Mayhew JE, Coffey PJ. Retinotopy within rat primary visual cortex using optical imaging. *Neuroimage* 24: 200–206, 2005.

Goldberg JH, Tamas G, Aronov D, Yuste R. Calcium microdomains in aspiny dendrites. *Neuron* 40: 807–821, 2003.

Hatsopoulos N, Gabbiani F, Laurent G. Elementary computation of object approach by a wide-field visual neuron. *Science* 270: 1000–1003, 1995.

Helmchen F, Imoto K, Sakmann B. Ca^{2+} buffering and action potential-evoked Ca^{2+} signaling in dendrites of pyramidal neurons. *Biophys J* 70: 1069–1081, 1996.

Helmchen F, Nägerl UV. Biochemical compartmentalization in dendrites. In: *Dendrites* (3rd ed.), edited by Stuart G, Spruston N, Häuser M. Oxford, UK: Oxford Univ. Press, 2016.

Homma R, Baker BJ, Jin L, Garaschuk O, Konnerth A, Cohen LB, Bleau CX, Canepari M, Djurisic M, Zeceivc D. Wide-field and two-photon imaging of brain activity with voltage- and calcium-sensitive dyes. *Methods Mol Biol* 489: 43–79, 2009.

Hopp E, Borst A, Haag J. Subcellular mapping of dendritic activity in optic flow processing neurons. *J Comp Physiol A* 200: 359–370, 2014.

Jones PW, Gabbiani F. Synchronized neural input shapes stimulus selectivity in a collision-detecting neuron. *Curr Biol* 20: 2052–2057, 2010.

Jones PW, Gabbiani F. Logarithmic compression of sensory signals within the dendritic tree of a collision-sensitive neuron. *J Neurosci* 32: 4923–4934, 2012.

Knudsen E, Konishi M. A neural map of auditory space in the owl. *Science* 200: 795–797, 1978.

Krahe R, Maler L. Neural maps in the electrosensory system of weakly electric fish. *Curr Opin Neurobiol* 24: 13–21, 2014.

Krapp HG, Gabbiani F. Spatial distribution of inputs and local receptive field properties of a wide-field, looming sensitive neuron. *J Neurophysiol* 93: 2240–2253, 2005.

Li D, Shao L, Chen BC, Zhang X, Zhang M, Moses B, Milkie DE, Beach JR, Hammer JA 3rd, Pasham M, Kirchhausen T, Baird MA, Davidson MW, Xu P, Betzig E. Extended-resolution structured illumination imaging of endocytic and cytoskeletal dynamics. *Science* 349: aab3500, 2015.

Nikolenko V, Watson BO, Araya R, Woodruff A, Peterka DS, Yuste R. SLM microscopy: scanless two-photon imaging and photostimulation using spatial light modulators. *Front Neural Circuits* 2: 5, 2008.

O'Shea M, Rowell CH. The neuronal basis of a sensory analyser, the acridid movement detector system. II. Response decrement, convergence, and the nature of the excitatory afferents to the fan-like dendrites of the LGMD. *J Exp Biol* 65: 289–308, 1976.

O'Shea M, Williams JL. The anatomy and output connection of a locust visual interneurone: the lobular giant movement detector (LGMD) neurone. *J Comp Physiol* 91: 257–266, 1974.

Peng H, Bria A, Zhou Z, Iannello G, Long F. Extensible visualization and analysis for multidimensional images using Vaa3D. *Nat Protoc* 9: 193–208, 2014a.

Peng H, Ruan Z, Long F, Simpson JH, Myers EW. V3D enables real-time 3D visualization and quantitative analysis of large-scale biological image data sets. *Nat Biotechnol* 28: 348–353, 2010.

Peng H, Tang J, Xiao H, Bria A, Zhou J, Butler V, Zhou Z, Gonzalez-Bellido PT, Oh SW, Chen J, Mitra A, Tsien RW, Zeng H, Ascoli GA, Iannello G, Hawrylycz M, Myers E, Long F. Virtual finger boosts three-dimensional imaging and microsurgery as well as terabyte volume image visualization and analysis. *Nat Commun* 5: 4342, 2014b.

Peron SP, Gabbiani F. Spike frequency adaptation mediates looming stimulus selectivity in a collision-detecting neuron. *Nat Neurosci* 12: 318–326, 2009.

Peron SP, Jones PW, Gabbiani F. Precise subcellular input retinotopy and its computational consequences in an identified visual interneuron. *Neuron* 63: 830–842, 2009.

Peron SP, Krapp HG, Gabbiani F. Influence of electrotonic structure and synaptic mapping on the receptive field properties of a collision-detecting neuron. *J Neurophysiol* 97: 159–177, 2007.

Quirin S, Jackson J, Peterka DS, Yuste R. Simultaneous imaging of neural activity in three dimensions. *Front Neural Circuits* 8: 29, 2014.

Rind FC, Simmons PJ. Orthopteran DCMD neuron: a reevaluation of responses to moving objects. I. Selective responses to approaching objects. *J Neurophysiol* 68: 1654–1666, 1992.

Santer RD, Rind FC, Stafford R, Simmons PJ. Role of an identified looming-sensitive neuron in triggering a flying locust's escape. *J Neurophysiol* 95: 3391–3400, 2006.

Schlotterer GR. Response of the locust descending movement detector neuron to rapidly approaching and withdrawing visual stimuli. *Can J Zool* 55: 1372–1376, 1977.

Schuett S, Bonhoeffer T, Hübener M. Mapping retinotopic structure in mouse visual cortex with optical imaging. *J Neurosci* 22: 6549–6559, 2002.

Shaw SR. Optics of arthropod compound eye. *Science* 164: 88–90, 1969.

Spalthoff C, Egelhaaf M, Tinnefeld P, Kurtz R. Localized direction selective responses in the dendrites of visual interneurons of the fly. *BMC Biol* 8: 36, 2010.

Strausfeld NJ, Nässel DR. Neuroarchitectures serving compound eyes of crustacea and insects. In: *Comparative Physiology and Evolution of Vision of Invertebrates B: Invertebrate Visual Centers and Behavior*, edited by Autrum H. Berlin: Springer, 1981, vol. I, p. 1–132.

Yaksi E, Friedrich RW. Reconstruction of firing rate changes across neuronal populations by temporally deconvolved Ca^{2+} imaging. *Nat Methods* 3: 377–383, 2006.